9

Review

Xavier X. Chia and Dawn T. H. Tan*

Deuterated SiNx: a low-loss, back-end CMOS-compatible platform for nonlinear integrated optics

https://doi.org/10.1515/nanoph-2022-0626 Received October 13, 2022; accepted January 31, 2023; published online February 13, 2023

Abstract: Silicon nitride (SiN) has surged into prominence as a material for photonic-integrated circuits (PICs) in the past decade, well regarded for its broadband transparency, compatibility with complementary metal oxide semiconductor (CMOS) fabrication processes and high optical bandgap that avoids two-photon absorption. However, current fabrication methods result in users having to choose between low thermal budgets and low losses, which are suboptimal given that both are necessary to facilitate a wide range of applications. Recently, works have emerged featuring PICs fabricated using deuterated silicon nitride (SiNx:D) - SiNx films grown using deuterated precursors instead of conventional hydrogenated ones. This decreases material absorption near the telecommunications bands at 1.55 µm previously present due to parasitic silicon-hydrogen and nitrogen-hydrogen bonds, attaining low-loss PICs realised using a low temperature, backend-of-line CMOS-compatible fabrication plasma-enhanced chemical vapour deposition process. These devices have shown promise for both linear and nonlinear applications and the platform has the potential to be instrumental in realising highly efficient chips with co-packaged electronics and photonics devices. This paper reviews recent developments on the SiNx:D platform and provides a glance at future advancements for this highly promising material.

*Corresponding author: Dawn T. H. Tan, Photonics Devices and Systems Group, Engineering Product Development, Singapore University of Technology and Design, 8 Somapah Road 487372, Singapore, Singapore; and Agency for Science, Technology and Research (A*STAR), Institute of Microelectronics, 2 Fusionopolis Way 138634, Singapore, Singapore, E-mail: dawn_tan@sutd.edu.sg. https://orcid.org/0000-0002-7111-1125

Xavier X. Chia, Photonics Devices and Systems Group, Engineering Product Development, Singapore University of Technology and Design, 8 Somapah Road 487372, Singapore, Singapore. https://orcid.org/0000-0002-0112-6110

Keywords: chemical vapour deposition; nonlinear optics; photonic-integrated circuits; silicon photonics.

1 Introduction and background

In the past decade of research in photonic-integrated circuits (PICs), silicon nitride (SiN) thin films have been a dominant material for the realisation of efficient passive devices. The applications of these films are ubiquitous – the material has been previously employed in areas such as the passivation of solar cells [1, 2], microstructures [3, 4] and membranes [5, 6] in micro-electromechanical systems (MEMs) long before their rise in popularity for C-band integrated optics. Over time, low-pressure and plasma-enhanced chemical vapour deposition (LPCVD/PECVD) methods have become fabrication methods of choice for depositing SiN thin films given their consistency and customizability, and it has become rare to see other methods used in their fabrication although some of these such as reactive [7] or magnetron sputtering [8] have emerged recently.

The study of the nonlinear optical properties of silicon nitride dates back to 2008, when Ikeda et al. investigated the thermal and Kerr nonlinearity in PECVD-grown SiN films and their use in photonic waveguides [9, 10]. Since then, optical devices implemented on silicon nitride have achieved a remarkable number of milestones over the years, most significant of which is their impact on microresonator frequency combs [11-20], spanning applications such as high-speed communications [21-25] and metrology [26-30]. The strength of the silicon nitride (SiN) platform lies in its broadband transparency and material compatibility with modern foundry processes [31], which has made SiN a popular platform for integrated optics with a growing number of groups advancing SiN technologies. Of note, the ultra-low losses achievable in LPCVD-grown silicon nitride that are thermally annealed at temperatures of up to 1200 °C have yielded ultralow losses as low as sub-dB/m [32-37], instrumental to the observations of nonlinear optical phenomena at low powers.

Aside from the study of SiN that is close to its stoichiometric composition for nonlinear optics, a separate effort in the study of tailoring the linear and nonlinear properties of SiNx films was taking place. Chemical vapour deposition techniques for growing SiNx films provide a design degree of freedom for compositionally tailoring SiNx films between silicon-rich or nitrogen-rich chemistries, effectively providing a sliding scale in the films' optical properties. In the fabrication of CVD silicon-nitride films, the Si:N ratios may be varied by controlling the ratios of the precursor gases used to provide the Si and N content in the films. Some common precursor gases used for supplying Si content include SiH₄ and SiH₂Cl₂, whereas precursor gases used to supply the N content include NH₃ and N₂ gas. It has been documented by various groups that tuning the precursor gas ratio to have a higher Si precursor gas flow rate may lead to silicon-rich nitride films with a higher linear and nonlinear refractive index [38-51]. In general, work in this area has aimed to achieve a maximum Kerr nonlinearity while retaining a sufficiently large material bandgap to preclude two-photon absorption at the telecommunications wavelength. For clarity, the abbreviation SiN shall henceforth be used to refer to films with Si:N ratios close to stoichiometric values (Si₂N₄), while SiNx will be used to refer to SiN and SRN in general.

In the domain of nonlinear optics, SiNx also possesses an advantage over silicon-on-insulator technologies through the avoidance of two-photon absorption (TPA) at telecommunications wavelengths due to their larger bandgap, which can range from 2.1 eV (Si₇N₃) [52] to 5 eV (Si₃N₄) depending on the Si:N ratio. In PECVD siliconrich nitride waveguides, Kerr nonlinearity above that of crystalline silicon devices have also been achieved while retaining a bandgap above the TPA threshold [47], which evidences the suitability of silicon-rich nitride as a more viable candidate than silicon in nonlinear integrated optics.

However, certain important drawbacks associated with CVD SiNx platforms limit the platform from becoming an ideal material. During deposition, silane (SiH₄) or dichlorosilane (SiH2Cl2 or DCS) is used as precursor gases to introduce silicon (Si) and nitrogen (N2) or ammonia gas (NH₃) for the nitrogen component, which results in the introduction of hydrogen content in the chamber. These hydrogen atoms are incorporated into the film, forming parasitic Si-H and N-H bonds that have infrared vibrational modes in regions around 2157 cm⁻¹ to 2250 cm⁻¹ and 3290 cm^{-1} to 3464 cm^{-1} , respectively [53–55]. While these do not directly impede the propagation of light in the C-bands,

they result in absorption overtones that peak near 1.52 µm and bleed into the region at the telecommunications bands near 1.55 µm. This absorption mechanism has been documented to limit the propagation losses in SiNx waveguides to roughly 1.5 dB/cm [44, 56]. This issue also tends to affect PECVD films more extensively as the low process temperature (ranging from 270 °C to 350 °C) results in considerable hydrogen bonds becoming incorporated within the films [57]. Some degree of success in reducing N-H related absorption has been achieved by replacing ammonia gas (NH₃) with nitrogen (N₂), but the remaining hydrogen content from Si-H bonds continues to cause deleterious losses at the important telecommunications wavelengths [58].

In response to SiNx material absorption from hydrogen containing bonds, the silicon photonics community has largely responded through the use of LPCVD deposition and high temperature annealing steps that eliminate the parasitic bonds in a high temperature environment of up to 1200 °C, such as in the photonic Damascene process [59, 60] or other related subtractive methods [35, 61]. While this has resulted in great strides in the improvement of silicon photonics technologies, the high temperatures make them less suitable for back-end-of-line (BEOL) complementary metaloxide semiconductor (CMOS) requirements, which tend to have a thermal budget between 400 °C and 525 °C. The manufacturing of commercial silicon photonics that include application specific integrated circuits include electrical interconnects in the lower layers, defined by many frontend-of-line (FEOL) processes. This is followed by low k- or copper-based metal interconnects followed by a photonics layer at the top. By this point in the process, any high temperature processes [62-64] employed to process the photonics layer at the top will negatively affect the electrical device layers defined on the front end, including dopant migration and melting of copper, which makes LPCVD silicon nitride that has a high thermal budget incompatible with BEOL processes.

More recently (as is the subject of this mini-review), we have seen an increase in popularity of deuterated silicon nitride (SiNx:D) - silicon nitride films deposited using deuterated silane (SiD₄) and N₂ gas, which removes hydrogen from the precursor gases entirely, importantly while maintaining low deposition temperatures below 400 °C. This has the effect of completely replacing Si-H and N-H bonds with Si-D and N-D bonds, which results in a change in infrared vibrational modes of the film by virtue of the isotopic shift. This change has profound implications, for it shifts the Si-H related bond absorption overtone at the 1.52 µm region to 2.1 µm (associated with Si-D), completely away from the entire telecommunications

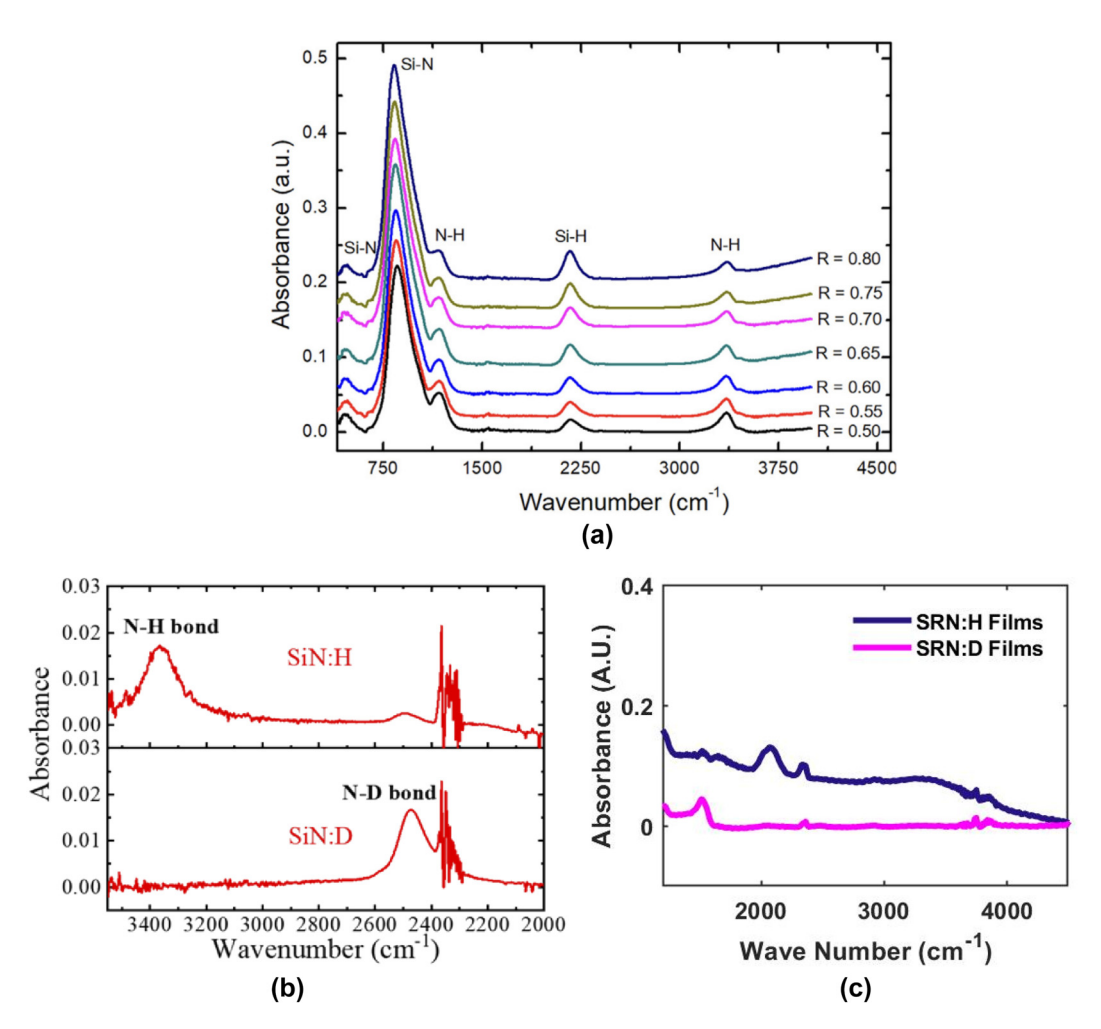


Figure 1: Fourier Transform Infrared (FTIR) spectra from various SiNx films in literature, showing infrared vibrational modes of constituent bonds. (a) FTIR data of PECVD SiNx:H films deposited with varying gas ratios. R is given as the ratio of SiH_a:(SiH_A + NH₃) used during deposition. Peaks corresponding to infrared vibrational modes of specific modes highlighted in the film, approximately located at 460 cm⁻¹, 840 cm⁻¹, 1170 cm⁻¹, 2160 cm⁻¹ and 3360 cm⁻¹ corresponding to Si-N symmetric stretching, Si-N asymmetric stretching, N-H wagging, Si-H stretching and N-H stretching modes, respectively. Figure adapted from [53]. (b) FTIR spectrum for SiNx:H and SiNx:D films, showing the absorbance locations associated with the N-H and N-D bonds [67]. (c) FTIR absorbance curve of PECVD SRN:D film versus SRN:H film. Bond regions where Si-H and N-H curves are expected noticeably empty in the SRN:D curves due to the lack of hydrogen atoms in the precursor gases used during deposition. Figure adapted from [51, 65].

band. Figure 1(b) and (c) show the infrared vibrational spectra obtained using Fourier-transform infrared spectroscopy (FTIR) of SiNx:H versus SiNx:D films, demonstrating the effects of substituting deuterium for hydrogen in the precursor gases. The mechanics of this phenomenon arise from changes in the vibrational bond energies [65], which are described using the quantum harmonic oscillator model and allow us to predict the shift in the absorption overtones [66]:

$$-\frac{h^2}{2m}\frac{d^2\psi}{dx^2} + \frac{1}{2}kx^2\psi = E\psi$$
 (1)

Here, h is Planck's constant, Ψ is the wave function, x is the displacement from equilibrium and E is energy. For the boundary conditions of $\Psi = 0$, $x = \pm \infty$, this generates the closed form expression for the vibrational bond energy as given by [26]:

$$E_{v} = h \cdot (1/2\pi) \cdot (v + 1/2) \sqrt{k/m_{1} + k/m_{2}}$$
 (2)

where v is the vibrational quantum number (an integer), k is the bond's force constant and $m_{1,2}$ is the atomic mass for the two atoms making up the bond. From Eq. (2), it is observed that variations in m_1 or m_2 will result in a change in the vibrational bond energy. In the case of SiNx:D, hydrogen atoms are substituted with deuterium, which retains the force constant of the bond while increasing the molecular mass, given that deuterium and hydrogen have an atomic mass of approximately 2 and 1, respectively. A substitution of deuterium for hydrogen thus gives rise to the shift in molecular absorption spectra also known as the isotope shift that pushes absorption regions away from the telecommunications bands near 1.55 µm [58].

The resulting SiNx:D devices achieve losses and resonator quality factors equivalent to unannealed LPCVD films [65, 68] and improvements in propagation losses across the telecommunications bands [56] while retaining back-end CMOS compatibility due to process temperatures. The PECVD-deposited films also have the advantage of a single-step deposition process not privy to LPCVD deposition methods that require additional process steps to circumvent high film stress such as the scoring of trenches or a multistage deposition process. Notably, LPCVD grown SiN films typically have high stress on the order of 1 GPa [48, 60] while a 568 nm thick ICPCVD SiN:D film was characterized by Chiles et al. [69] to possess film stress of 191 MPa.

The advantage of SiNx:D lies in that it combines the advantages of PECVD and LPCVD SiNx:H, yielding films with high refractive index, high nonlinearity, low losses and low film stress in a convenient single-step deposition method. This circumvents the strict trade-off of low losses or CMOS compatibility that users of the SiNx platform have had to reckon with thus far. Since their introduction in 2017 [56], SiNx:D PICs have experienced intensified interest, being involved in a number of works including ultralow-loss CMOS-compatible waveguiding devices, frequency comb generation and soliton generation. In the subsequent sections, we will cover recent advancements in SiNx:D devices in both the linear and nonlinear domains. The work then concludes with a brief section on the future outlook for these devices.

2 Recent work in linear optics

The first effective demonstration of SiN:D waveguides was presented by Hiraki et al. in 2017 [56]. In this work, an SiN:D film was fabricated via electron-cyclotron-resonance PECVD (ECR-PECVD) at 200 °C using SiD₄ and N₂ gas as the precursor gases. The resulting film possessed a refractive index of 1.87 at 1550 nm and 1.8 cm long waveguides with a cross section of 0.55 μ m \times 1.1 μ m (height \times width) fabricated on the film showed a TE₀₀ mode propagation loss of 0.47 dB/cm. Reference SiN:H films fabricated using the same deposition process yielded hydrogen contents almost 20 times higher than the SiN:D film, evidencing the effectiveness of hydrogen reduction in improving material absorption losses. When benchmarked against devices fabricated on SiN:H films, the SiN:D devices presented significant improvements in transmission in the wavelength range from 1.4 μ m to 1.6 μ m.

The use of SiN:D as an optical platform has gained significant traction since then, inspiring a number of works [67, 69-71] that leverage the advantages afforded by the material and fabrication process. In contrast with low-loss LPCVD SiNx:H waveguides that required multi-stage processes including deposition, the use of trenches to alleviate high stress and high temperature annealing, advancements in SiNx:D research have yielded devices with increasingly lower losses that can be realised using a simple single-stage deposition (Figure 2). Micro-ring resonators (MRRs) with intrinsic quality factors up to 1.2 million [72] and devices with losses as low as 0.17 dB/cm [67] have since been demonstrated. In these works, the SiN:D films were deposited via Inductively-Coupled Plasma CVD (ICPCVD - a high-density plasma variant of PECVD) at 270 °C, resulting in films with a refractive index of ~1.99 at 1550 nm and a film thickness of 880 nm. The resulting devices were ideal candidates for frequency comb generation given the relatively higher nonlinearity compared to silicon-dioxide and anomalous dispersion afforded by the thick SiN:D layer and will be covered more in-depth in the following section on nonlinear optics.

Propagation losses in waveguides can be further reduced through the use of SiD₄ gas in the fabrication of the SiO₂ cladding, forming a waveguide with a SiN core and SiO2 cladding grown entirely with precursor gases containing deuterium instead of hydrogen (Figure 2). Jin et al. documented a comparison between SiO2 thin films grown using SiH₄ and SiD₄ [73]. The use of SiD₄ gas instead of

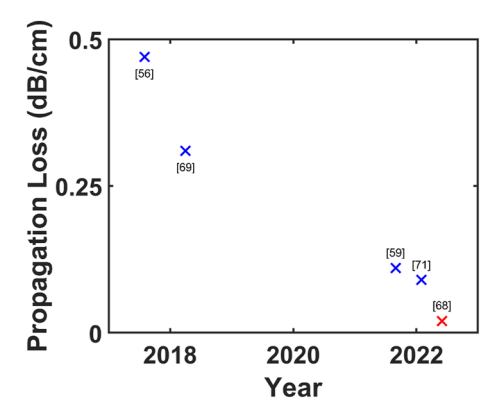


Figure 2: Table showing progressive improvements in propagation loss performance for SiN:D devices reported in literature. Blue crosses (x) indicate loss values achieved with devices using high modal confinement while red crosses (x) denote low modal confinement where significant amounts of power of the propagating mode is located within the cladding. In general, waveguide geometries with lower modal confinement have lower susceptibility to sidewall roughness and associated losses, while high modal confinement geometries exhibit stronger nonlinear properties.

SiH₄ shifts the first absorption overtone of SiO-H from 1390 nm to 1870 nm in SiO-D, well outside the telecommunications band. Figure 3(a) shows the measured absorbance for both films, obtained using Fourier transform infrared spectroscopy. It is observed that the deuterated SiO₂ films possess significantly lower absorbance for wavenumbers between 3300 and 3700 cm⁻¹, which correspond to the fundamental SiO-H absorption. Conversely, higher absorbance is observed for wavenumbers between 2600 and 2700 cm⁻¹, corresponding to the fundamental SiO-D absorbance. The use of deuterated SiO₂ cladding is of particular importance for waveguide devices, which are weakly confined (and equivalently have a large effective area), as a significant part of the electric field would reside in the cladding and be subjected to attenuation from material losses. At the same time, low confinement waveguide geometries (such as those shown in columns 1 and 3 of Table 1) are an excellent approach to achieving extremely low-loss waveguides due to lowered susceptibility to sidewall roughness and its associated losses. In such waveguides, the evanescent tails of the mode extend considerably into the cladding, and the interaction of the mode with the waveguide sidewalls that are subjected to fabrication induced roughness will be very small. This limits the impacts of scatteringrelated losses in the propagating modes. Such waveguides were first studied in non-deuterated, LPCVD grown silicon nitride, cladded with deuterated SiO₂ cladding. Around 8-9 dB/m losses in waveguides with a width and height of 2.8 µm and 80 nm-100 nm, respectively, were achieved [32]. These were then extended to similarly low confinement waveguides incorporating deuterated silicon dioxide cladding, where losses in similarly sized waveguides were demonstrated to decrease to 5 dB/m [73]. It may be observed from Figure 3(b) that a 30-fold loss reduction is enabled by the deuterated precursor gas at a wavelength of 1400 nm (300 dB/m to 10 dB/m), whereas optical frequency domain reflectometry measurements reveal a reduction in the propagation losses from 8 dB/m to 3 dB/m at 1550 nm.

The aforementioned work reaped the benefits of a deuterated SiO2 cladding but did not fully take advantage of the deuterated process for the silicon nitride waveguide core. More recently, silicon nitride waveguides (cross section 6 μ m \times 80 nm) were fabricated with deuterated

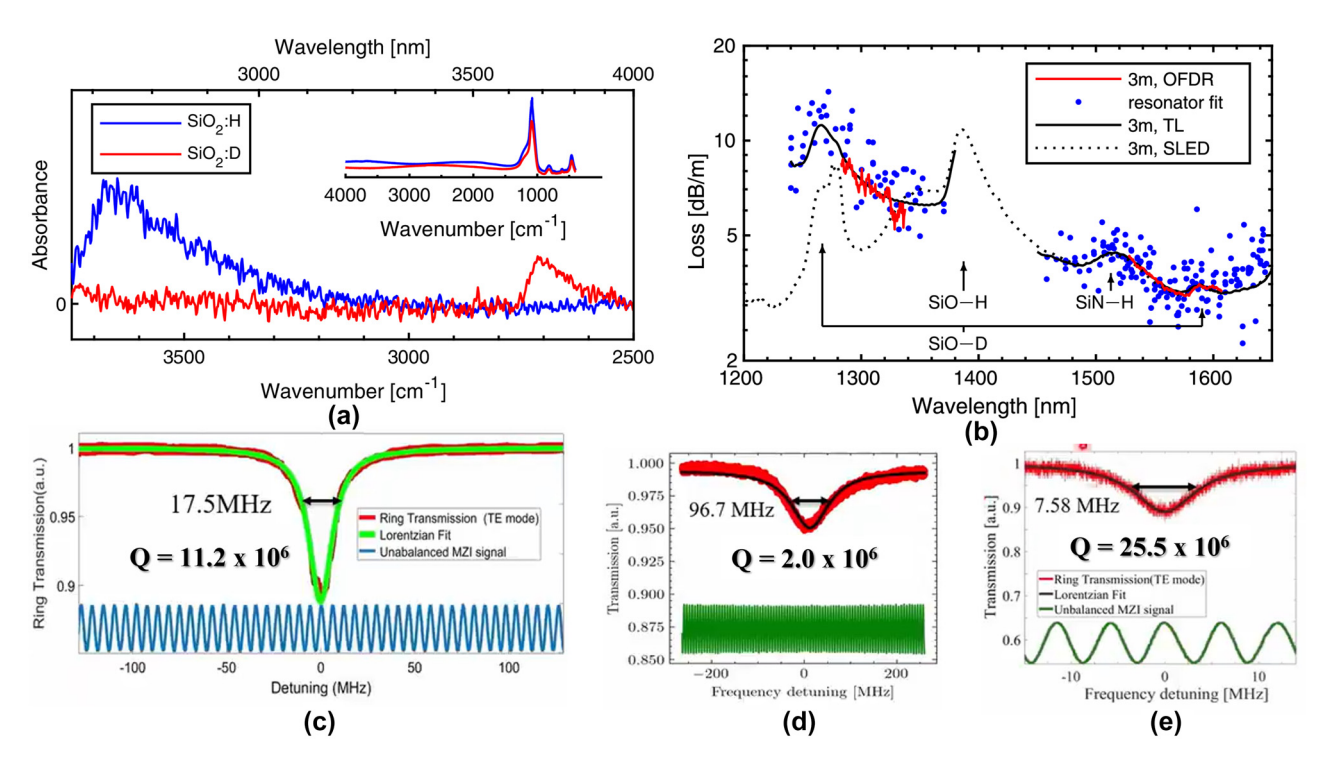


Figure 3: FTIR measured absorbance of SiO₂:H and SiO₂:D thin films, which results in a shift in the fundamental SiO-H vibrational mode at 2.73-3.74 μm for SiO – D. The inset shows the FTIR spectrum in an extended range. (b) Measured waveguide losses for SiN waveguides with SiH₄-grown and SiD₄ grown SiO₂ cladding. The losses were measured using super luminescent light emitting diode transmission measurements and OFDR measurements. Measured MRR resonator transmission and loaded quality factor for (c) SiD₄ grown SiN core, (d) 800 °C LPCVD SiN core, (e) 800 °C LPCVD SiN core annealed at 1050 °C for 7 h. MRRs in (c), (d) and (e) used an SiO₂ cladding grown using SiD₄. (a) and (b) are from Ref. [73]. (c)–(e) are from Ref. [68].

Table 1: Properties of SiNx films reported in literature.

Parameters	Sil	SiNx:D	
Deposition type	LPCVD	PECVD	PECVD
Lowest recorded propagation loss @ 1.55 µm (waveguide dimensions in W × H, propagating mode)	Very low (annealed) 0.034 dB/m [74] (11 μm × 800 nm, TM mode)	Fairly high 1.5 dB/cm [44] (1.5 μ m $ imes$ 300 nm, TE mode)	Low 2.0 dB/m [68] (6.0 μ m \times 80 nm, TM mode)
Ease of fabrication	Multi-stage deposition/annealing required to achieve thicker films	Single step	Single step
Back-end CMOS compatible	No, exceeds thermal budget (>450 °C)	Yes	Yes
Highest reported refractive index Highest reported nonlinear parameter, Kerr nonlinearity	2.2 [45] $6 \text{ W}^{-1} \text{ m}^{-1}$, $1.1 \times 10^{-18} \text{ m}^2/\text{W}$ [45]	3.1 [52] 550 W ⁻¹ m ⁻¹ , 2.8 × 10^{-17} m ² /W [52]	2.5 [65] 95 W ⁻¹ m ⁻¹ , 9.8 \times 10 ⁻¹⁸ m ² /W [65]
Film stress (deposited thickness)	~1 GPa (N.D.) [60]	316 MPa (255 nm) [48]	191 MPa (568 nm) [69]

N.D., no data.

silane for both the silicon nitride core and SiO₂ cladding, yielding waveguides with losses as low as 2 dB/m and ring resonators with a loaded quality factor Q_L of 11.2 million (Figure 3(c)) for the quasi-TE mode at 1550 nm [68]. In the same work from Bose et al., the performance of the SiN:D/SiO₂:D devices were compared to hybrid SiN devices. These hybrid devices were fabricated using an 800 °C LPCVD-deposited SiN:H core and 250 °C PECVD-deposited SiO₂:D cladding, and comparisons in performance showed a small improvement to 1.57 dB/m but a six-fold decrease in the $Q_{\rm L}$ to 1.98 million (Figure 3(d)). When using 800 °C LPCVD SiN annealed for 7 h at 1050 °C with deuterated SiO₂ cladding, the waveguides outperformed the SiN:D/SiO₂:D devices, attaining losses of 1.00 dB/m and a $Q_{\rm L}$ of 25.5 million (Figure 3(e)). This study provides a comparison of the losses in the various core and cladding materials and shows that deuterated silane provides an avenue for ultra-low-loss waveguides, on the order of dB/m, which is sufficient for most applications.

While the nonlinear parameters of these propagating modes are inevitably lower due to low modal confinement and are thus not ideal for nonlinear optical applications, these devices are prime candidates for applications requiring very low losses such as use as waveguide interconnects for information carriers, gyroscopes and optical reference cavities [77]. These works ultimately show that the substitution of hydrogen for deuterium in the deposition of silicon nitride films makes for a highly effective single-step deposition process for the creation of very low-loss, back-end CMOS-compatible integrated optical devices.

3 Recent work in nonlinear optics

Apart from generating low-loss waveguides, SiN:D is currently being studied with great interest for nonlinear optics. This endeavour differs from the fabrication of ultra-low-loss devices in the previous section, which focused on the design goal of the lowest possible losses, a key approach being the exploitation of weakly confined waveguide modes using a thin waveguide core. In nonlinear optics applications, low losses are important, but not the only variable in the equation. Both the Kerr nonlinearity (n_2) of the waveguide and the modal profile play a strong role in the resulting efficiency of nonlinear phenomena. Nonlinear dynamics in photonic devices may be described using the nonlinear Schrödinger equation [78]:

$$\frac{\partial A}{\partial z} = -\frac{\alpha}{2}A + i\sum_{k=2}^{\infty} \frac{i^k}{k!} \beta_k \frac{\partial^k A}{\partial T^k} + i\gamma (|A|^2 A)$$
 (3)

where z is the longitudinal coordinate and α is the linear loss coefficient. A, T and β_k are the slow varying pulse envelope, time and dispersion of kth order, respectively. The nonlinear parameter, $\gamma=\frac{2\pi n_2}{\lambda A_{\rm eff}}$, where λ is the wavelength, and $A_{\rm eff}$ the effective modal area of the propagating mode. γ in particular is a strong contributor to many nonlinear effects leveraging the 3rd order nonlinearity of a material, including Four-Wave Mixing (FWM), broadband frequency comb and supercontinuum generation, self-phase modulation and optical amplification. In resonant structures such as the prolific microring used for frequency comb generation, nonlinear dynamics may be described using the Lugiato-Lefever

equation, interpreted as the damped and driven nonlinear Schrodinger equation [79]:

$$T_{R} \frac{\partial}{\partial T} A = -\left(\frac{\alpha}{2} + i\delta\right) A + i \sum_{k>1} \frac{\beta_{k}}{k!} \left(i \frac{\partial}{\partial t}\right)^{k} A$$
$$-j\gamma |A|^{2} A + \sqrt{\theta} A_{\text{in}} \tag{4}$$

where A is the envelope of the electric field, β_k describes the dispersion of kth order, T_R is the round-trip time in the microresonator, α is the round-trip loss, T and t are the slow and fast times respectively, δ is the detuning between pump and closest resonance, θ is the resonator-waveguide coupling coefficient and $A_{\rm in}$ is the continuous wave input. The equation accounts for the driving effect from the pump and the damping effect from dispersion and may be viewed as a modified version of the nonlinear Schrödinger equation used to describe nonlinear pulse propagation, with a key difference being the driving term represented by A_{in} .

As may be observed from both Eqs. (3) and (4), that γ plays an important role in the nonlinear optical phenomena. A larger nonlinear parameter lowers the amount of power required to observe waveguide-based nonlinear optics such as supercontinuum generation. In resonant-enhanced nonlinear optics, it similarly enables a reduction in the threshold power required for frequency comb generation, an area of research that currently has significant momentum in the field. For a fixed wavelength, improvements in the nonlinear parameter can be achieved by either (1) increasing the Kerr nonlinearity of a material or (2) decreasing the effective modal area of the propagating mode. In the case of SiNx devices, both of these occur when the silicon content in the films is increased, which can be engineered by increasing the ratio of silicon to nitrogen carrier precursor gases during CVD.

3.1 SiN:D Kerr frequency combs

The utility that frequency combs (FCs) have provided for the field of optics is indisputable, seeing use in applications such as high precision metrology [80], spectroscopy [81] and optical sources [21, 82]. Originally associated with the generation of mode-locked lasers, the generation of Kerr-microcombs in minute optical cavities such as Whispering Gallery Mode (WGM) resonators and planar-integrated MRRs has been a dominating branch of research in the community for the past 15 years. The first demonstration of Kerr frequency combs in a microscopic optical cavity was presented in 2007 [83]. Since then, significant progress has been made in microresonator-based Kerr frequency combs, which are planar in nature [11, 84-86].

Of intense interest is the generation of Dissipative Kerr Solitons (DKSs) [13, 19, 87] and the formation of temporally ordered micro-resonator soliton crystals [20, 88] - coherent, self-reinforcing pulses of light that result from a balance between dispersion and nonlinearity – in planar-integrated microcavity devices, which possess immense potential in space-sensitive applications such as portable light detection and ranging (LIDAR) devices [89]. Advancements in portability and miniaturisation have also seen these devices go from requiring the use of extensive table-top experimental setups to battery-powered comb generators [90], and SiN:D devices stand to make these technologies more easily accessible given their ease of fabrication and desirable optical properties.

Advancements in SiN:D technologies have largely followed this trend in micro-resonator research - in recent works, SiN:D devices have been frequently employed in the generation of broadband frequency combs (Table 2), with successive works improving in losses and exhibiting different comb characteristics. Modulational instability (MI) frequency combs in SiN:D MRRs were first demonstrated by Chiles et al. in 2018 [69]. In this work, the films were deposited using ICPCVD at a substrate temperature of 270 °C and chamber pressure of 10 mTorr, using SiD4 and N₂, resulting in 860 nm thick layers and a series of ring resonators realised using electron-beam lithography and an ICP-based reactive ion etching process. The resonators possessed waveguide cross sections of 1.5/1.6/2.1 μ m \times 0.86 μ m (width \times height) and identical ring radii of 23 μ m, featuring quality factors as high as 1.6×10^6 . Notably, the films were characterized to have low tensile stress (191 MPa for 568 nm thick films). Conversely, LPCVD grown SiN films typically have high stress on the order of 1 GPa [48, 60], which necessitates the use of stress management techniques such as multi-step deposition methods used in the photonic damascene process or proper definition of trenches homogenously throughout the entire wafer in order to achieve thick films that are required to achieve anomalous dispersion. This is in addition to the very high thermal budgets required of up to 1200 °C, where most processes use a 2- to 3-hour anneal time and some perform annealing after each of the multi-stage deposition steps. In contrast, films required for SiN:D devices possessing anomalous dispersion can be deposited in a single-step deposition process without the need for additional annealing, which has the additional benefit of preserving back-end CMOS compatibility.

The MI comb spectra was achieved at a coupled pump power of 440 mW, obtaining a wide spectrum spanning 1350 nm to 1900 nm ring widths of 1.5 μ m and 1.6 μ m while

Table 2: List of SiN:D works presenting MRR frequency combs including their optical properties, comb types and pump schemes.

Waveguide core dimensions (W \times H)	Propagation loss	Quality factor	Pumping configuration	Pump power	Comb type	Work, year
2.3μ m × 0.92 μ m	0.31 dB/cm	1.6×10^6 , loaded	Single pump	440 mW	Modulational instability	[69], 2018
$2.0 \mu m \times 0.88 \mu m$	0.17 dB/cm	2.29×10^6 , loaded	Single pump	100 mW	Perfect soliton crystals	[67], 2021
$1.8~\mu m \times 1.0~\mu m$	Not disclosed	0.8×10^6 , loaded	Auxiliary assisted	400 mW (Aux) 500 mW (main)	Single soliton	[75], 2022
$2.2~\mu\text{m}\times0.85~\mu\text{m}$	0.09 dB/cm (TE)	0.5×10^6 , loaded (TM) 0.65×10^6 , intrinsic (TM)	Auxiliary assisted	190 mW (Aux)	Single soliton	[70], 2022
				<220 mW (main)		
		1.5×10^6 , loaded (TE) 2.0×10^6 , intrinsic (TE)				

the resonator with a ring width of 2.1 µm exhibited comb spectra spanning 1200 nm-2100 nm. Importantly, the considerably wider generated comb spectrum for a ring width of 2.1 µm may be attributed small dispersion magnitude (inset of Figure 4(e)) over a wide bandwidth, facilitating efficient phase matching. While soliton steps were observed in the measured spectra (Figure 4(d)), stable soliton generation was not achieved in this work, with the authors citing strong thermal shifts in the resonance due to a larger absorption coefficient compared to annealed LPCVD SiN films. It is also worth noting that the already low propagation losses of 0.31 dB/cm are observed to be the highest recorded propagation loss values for SiN:D devices employed in the generation of frequency combs thus far.

Since MI combs in SiN:D MRRs were demonstrated by Chiles et al., frequency combs generated on the SiN:D platform have seen improvements in required pump power and comb coherence. Using SiN:D films grown using ICPCVD at a low temperature of 270 °C, Wu et al. [67] demonstrated MRRs with losses as low as 0.17 dB/cm and a loaded quality factor of 0.95 million. They also demonstrated microdisk resonators with a loaded quality factor of 0.7 million on the same platform [71]. Using SiN:D MRRs of various designs, perfect soliton crystals requiring coupled pump powers of only 13.5 mW for optical parametric oscillation and 100 mW for comb generation were demonstrated. Figure 5(a) shows the transitions from the Turing state (I) to the modulation instability state (II, IV and V), which is typically incoherent and noisy. The generated frequency combs corresponding to each of these detuning values are shown in Figure 5(b) and (d). The detuning corresponding to state III generates a soliton crystal state shown in Figure 5(c) to possess low RF noise. Soliton crystals were generated by driving a single pump laser into the blue-detuned regions of the resonance with a sweeping rate of 20 nm/s, attaining 7-PSC and 9-PSC results (combs with spacings 7 times

and 9 times the free-spectral range) in different devices (Figure 5(e) and (f)). However, while the soliton crystal states can be stably accessed with a number of different devices, the stability of the crystal does seem to be intermittent given that they break with other reported soliton crystal dynamics. The crystal states are shown to revert to incoherent MI comb states with further pump detuning, diverging from previously reported dynamics observed in simulations using the Lugiato-Lefever equation where solutions leading to PSC comb generation lies beyond the MI comb region [20].

Most recently in 2022, SiN:D MRRs have also been employed in the generation of highly coherent single-soliton frequency combs [70, 75]. Figure 6 shows the experimental setup and sech² spectra associated with single-soliton generation from [70] (Figure 6(a)) and [75] (Figure 6(b) and (c)), respectively, achieved with ring resonators of various ring radii. Notably, both works achieved single-soliton generation with the use of auxiliary lasers as described in [91], which differs from prior experimental schemes for soliton generation (single soliton or otherwise) [13, 92, 93] where a single pump laser was employed. DKSs are then generated by avoiding delayed thermo-optic effects through a judicious selection of the laser sweep rate. The auxiliary pump scheme is designed to mitigate these thermal dragging effects by coupling an auxiliary laser into another resonance, which relaxes the sweeping conditions required for the realisation of solitons by keeping cavity temperature relatively unchanged when the pump laser is shifted to the red-detuned region of the resonance. This setup is significantly more complicated and may speak towards the higher thermal susceptibility compared to LPCVD SiNx:H that was previously reported in [69]. Nonetheless, generating these solitons also usually require devices that have low thermal susceptibility such that mode locking can be sustained, which meant that these nonlinear phenomena were not

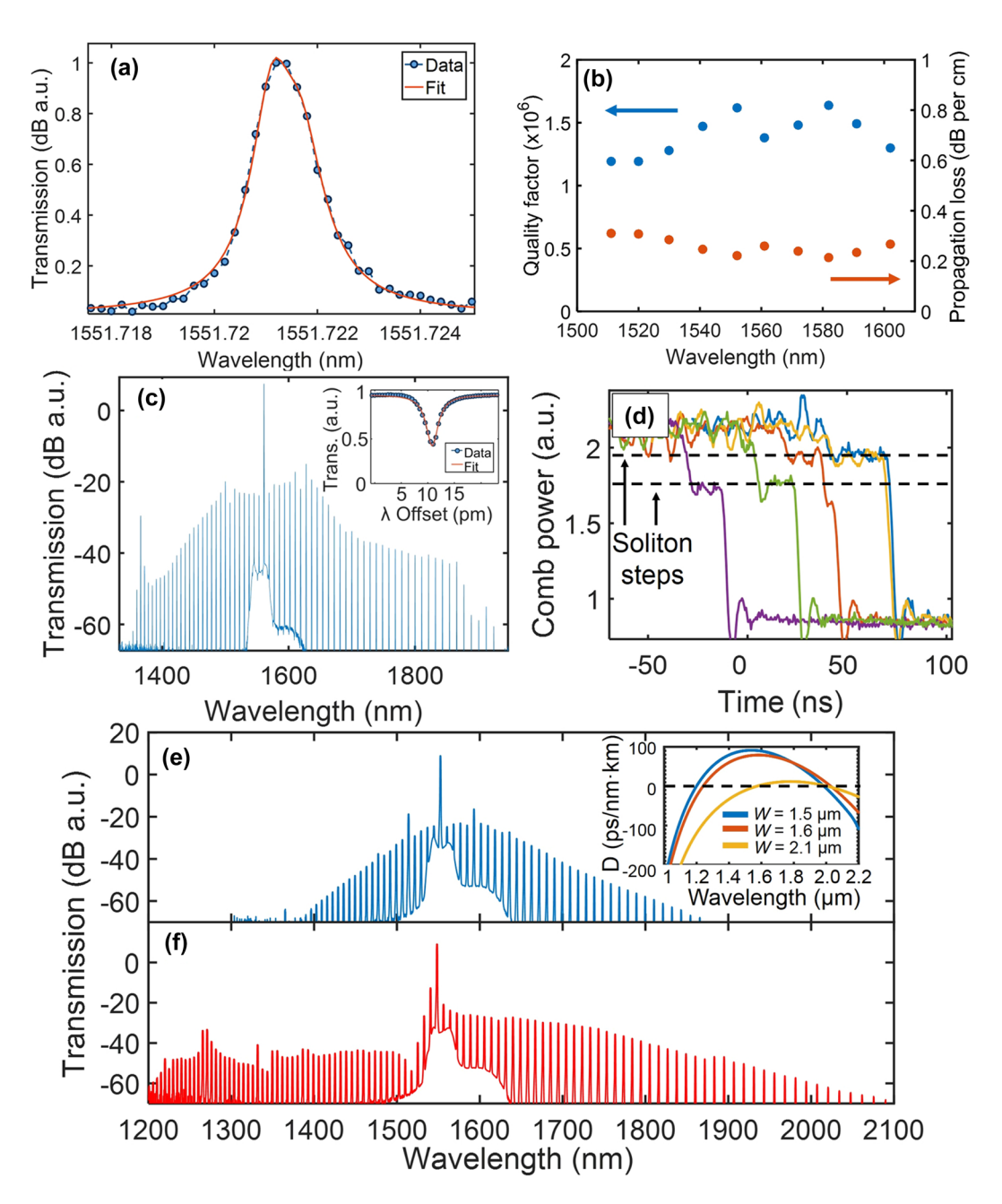


Figure 4: Optical characterization of a microring resonator fabricated using deuterated silicon nitride. (a) Transmission spectrum of the quasi-TE resonant mode at the drop port located at 1552 nm. (b) The measured quality factor and corresponding propagation loss as a function of wavelength. (c) Frequency comb spectrum generated from a microresonator with a width and height of 1.5 µm and 900 nm, respectively. The inset shows the resonant mode used to generate this comb with loaded Q of 5.6×10^5 . (d) Measured comb power (using an oscilloscope) during repeated red detuning of the pump laser frequency, showing evidence for dissipative Kerr-soliton transient formation with two discrete and repeatable step levels. The generated frequency comb for ring widths of (e) 1.6 and (f) 2.1 µm. The inset in (e) shows the numerically calculated dispersion for the zeroth order TE mode for widths of 1.5, 1.6 and 2.1 μm . Adapted from [69].

previously privy to PECVD SiNx:H films that featured higher hydrogen concentrations and absorption losses.

The successful realisation of PSCs and DKSs on the SiN:D marks its promise as a simple, low-loss, backend CMOS-compatible material platform nonlinear optical applications and unlocks nonlinear phenomena previously available only to high temperature annealed LPCVD SiN:H films. LPCVD SiN:H MRRs presently outperform SiN:D MRRs in terms of loss performance - the demonstration of octavespanning frequency combs in SiN:H MRRs in 2011 [12] employed an MRR with a quality factor of 3 million, outperforming the present state-of-the-art SiN:D MRR at 2.3

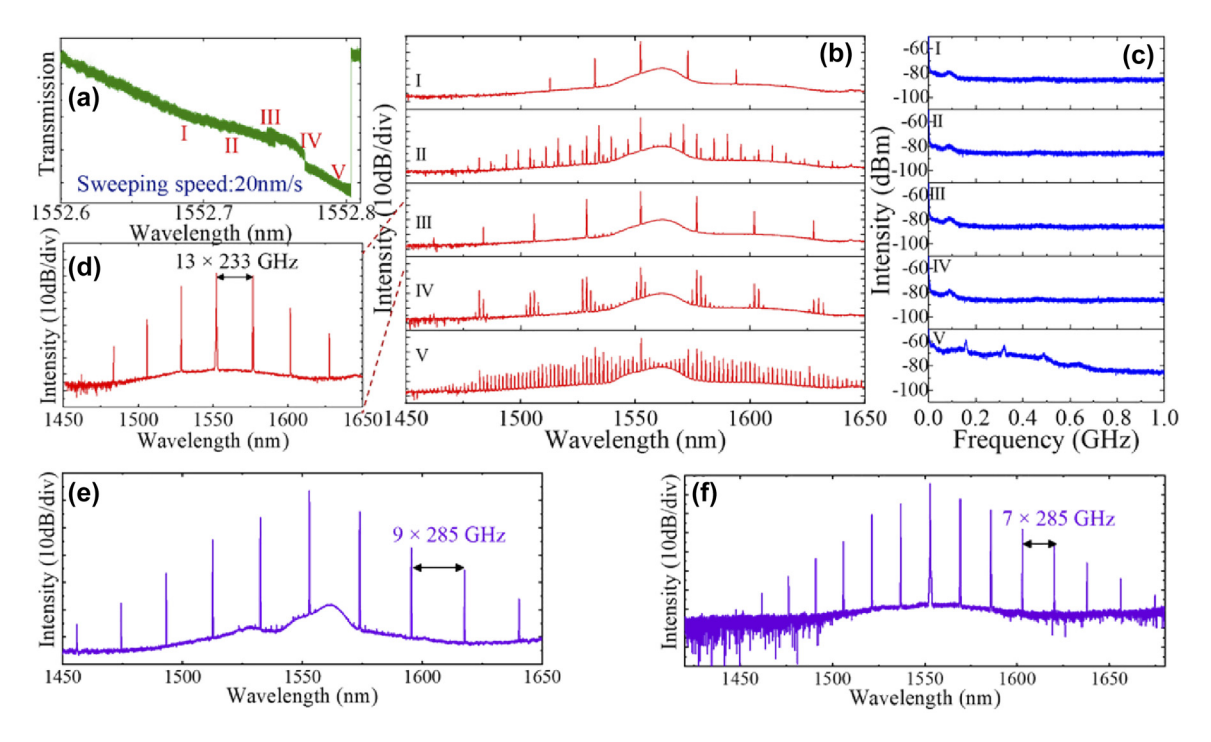


Figure 5: Experimental results of Turing and Perfect Soliton Comb (PSC) states realised on an SiN:D microresonator. (a) Pump transmission as a function of 100 mW for a SiN:D microring resonator with 100 μm radius and on-chip power of ~100 mW. (b) Frequency comb states and (c) intensity noise corresponding to the wavelengths denoted in (a). (d) Soliton crystal state III with ASE noise filtered out (zoomed in), prior to coupling into the waveguide. Spectral trace of (e) 9-PSC and (f) 7-PSC soliton combs [67].

million. In general, the high confinement resonators (which frequency combs fall under to meet anomalous dispersion requirements) fabricated on annealed LPCVD SiN:H have quality factors on the order of 10^6-10^7 [94, 95], though these authors have also stated that they have spent many years developing detailed process refinements to achieve such low losses. SiN:D is an emerging field, nascent compared to LPCVD SiN:H for photonics where the first papers on it were published in 2011 and is inevitably much more technologically mature. The fact that the best SiN:D resonators today are only about 10 times smaller in quality factor compared to the much more established LPCVD SiN:H shows that with time and the relevant process improvements, further increases in quality factor could be on the horizon (Table 3). In addition, the reduction in fabrication complexity and the potential of integrating BEOL processes with SiNx:D provides a promising outlook, and future improvements to fabrication processes might bring the loss performance of SiN:D devices down even further.

3.2 SiNx:D Kerr nonlinear optics

The nonlinear domain in integrated optics is usually accessible with a sufficiently high combination of light intensity and device nonlinearity. For example, optical parametric oscillations (OPOs) require a minimum threshold power before they are observed, and in fundamental 3rd order nonlinear effects such as Four-Wave Mixing (FWM) and Self-Phase Modulation (SPM), the nonlinear efficiency increases with the Kerr nonlinearity of the medium. When considering the integration of technologies into real-world systems, however, power consumption remains a core consideration due to concerns regarding cost and portability, which drives a never-ending pursuit for more efficient systems.

In the case of silicon nitride, the manipulation of the Si:N ratio of the film can lead to a variation in its physical and optical properties including film stress, photoluminescence refractive index amongst others [53, 96, 97]. Most importantly for nonlinear optics, an increase in silicon content also contributes to an increase in refractive index, which increases the nonlinearity of the film by virtue of Miller's rule [98-100]:

$$n_0 = \left(1 + \chi^{(1)}\right)^{\frac{1}{2}} \tag{5}$$

$$n_2 = \frac{3}{8n_0} \chi^{(3)}$$
 (6)
$$\chi^{(3)} \propto (\chi^{(1)})^4$$
 (7)

$$\chi^{(3)} \propto \left(\chi^{(1)}\right)^4 \tag{7}$$

Here, n_0 is the linear refractive index, $\chi^{(i)}$ is the *i*-th order electric susceptibility of the waveguiding media and

Table 3: SiNx:D works reported in literature for integrated optics including process conditions and optical properties of films and devices.

<i>n</i> @ 1550 nm	Gas flow rates	Pressure	Temp	RF power	ICP power	CVD type CVD type	Waveguide core dimensions (W $ imes$ H)	Propagation loss @ 1550 nm	Resonator quality factor	Work, year
1.87	40 sccm SiD4, 10 sccm Ar. 100 sccm N2	N.D.	200 °C	N.D.	N.D.	ECR-PECVD	1.1 µm × 0.55 µm	0.47 dB/cm	Not applicable	[56], 2017
1.98	36 sccm SiD4, 31 sccm N2	10 mTorr	270 °C	W 0	1000 W	ICPCVD	2.3 µm × 0.92 µm	0.31 dB/cm	1.6×10^6 , loaded	[69], 2018
1.99	N.D.	N.D.	270°C	N.D.	N.D.	ICPCVD	2.0 µm × 0.88 µm	0.17 dB/cm	2.29×10^6 , loaded	[67], 2021
1.95	N.D.	N.D.	250°C	N.D.	N.D.	ICPCVD	6.0 µm × 80 nm	2.23 dB/m (TE) 2.04 dB/m (TM)	11.18 \times 10 ⁶ , loaded (TE) 4 16 \times 10 ⁶ loaded (TM)	[68], 2022
1.95	N.D.	N.D.	200 °C	N.D.	ı	ECR-PECVD	1.8 µm × 1.0 µm	Not disclosed	0.8×10^6 , loaded	[75], 2022
1.96	N.D.	N.D.	270 °C	N.D.	ı	ICPCVD	2.2 µm × 0.85 µm	0.09 dB/cm (TE)	0.5×10^6 , loaded (TM)	[70], 2022
									0.65 × 10 ⁶ , intrinsic (TM) 1.5 × 10 ⁶ , loaded	
									(1E) 2.0 × 10°, intrinsic (TE)	
2.46	N.D. SiD4:N2 ratio 3:250	N.D.	350°C	N.D.	ı	PECVD	$5.0\mu\mathrm{m} \times 0.31\mu\mathrm{m}$	1.5 dB/cm	6.2×10^4 , loaded (TE)	[65], 2022
2.34	N.D. SiD4:N2 ratio 2:250	N.D.	350 °C	N.D.	ı	PECVD	2.0 µm × 0.35 µm	N.D.	1.27×10^5 , intrinsic (TE)	[76], 2022
2.52	N.D. SiD4:N2 ratio 4:250	N.D.	3€0 °C	N.D.	ı	PECVD	$2.0 \mu m \times 0.32 \mu m$	N.D.	1.18×10^5 , intrinsic (TM)	[76], 2022
N.D., not disclosed	sclosed.									

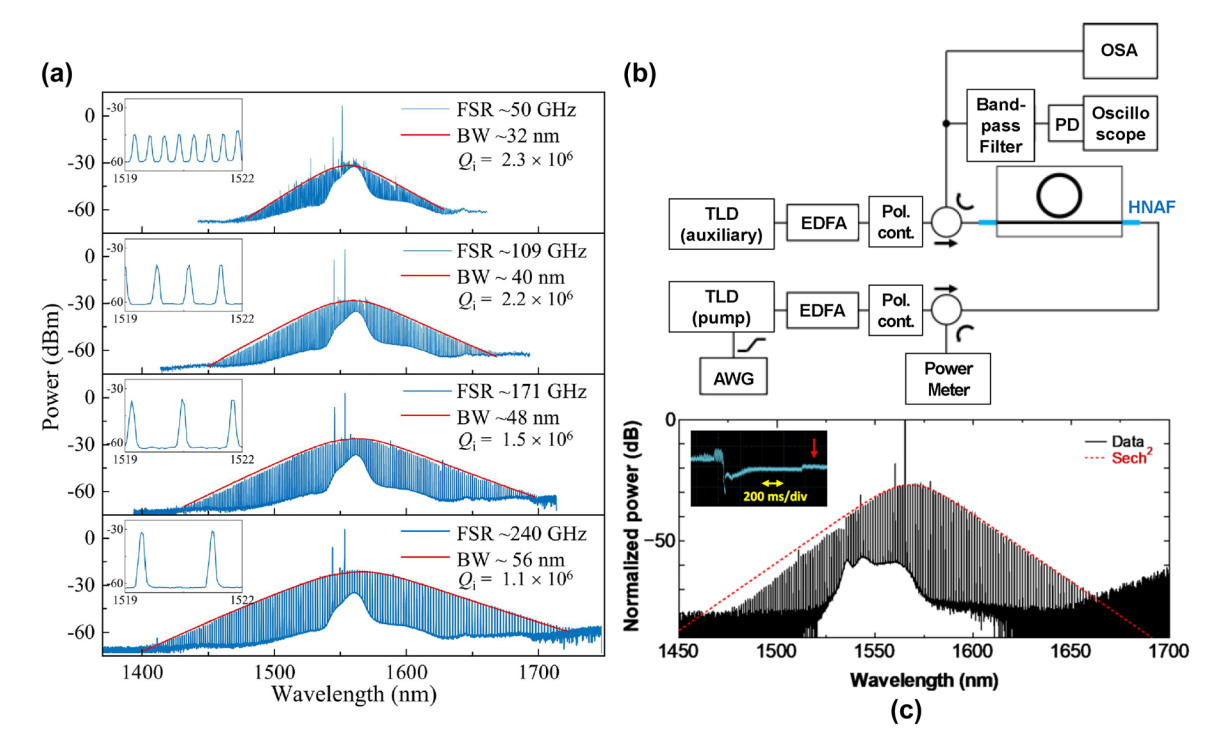


Figure 6: Single-soliton generation in SiN:D MRRs with different free spectral ranges. Figures show measured optical spectra (—) and sech² fit (—) characteristic of singly generated DKSs in MRRs of different radii, corresponding to different FSRs observed in the plot. This experimentally confirms that the platform is stable enough to facilitate single-soliton generation, a feature not seen in PECVD SiN:H MRRs thus far due to high material absorption near 1.55 µm as a result of parasitic hydrogen bonds. Consistent presence of two peaks in the spectrum arises from a dual-pump scheme described in [54] that suppresses relatively slower thermal dragging effects, relaxing the strict constraints of the scan speed required in previous single-pump schemes. Figure adapted from [70]. (b) Auxiliary laser setup used to generate the single-soliton comb state and (c) measured optical spectrum. Inset shows transmittance during laser wavelength sweep. (b) and (c) adapted from [75].

 n_2 is the material Kerr nonlinearity. The increase of n_2 in turn leads to an equivalent improvement of the nonlinearity experienced by the propagating mode within the waveguide that results in greater efficiency in the generation of nonlinear effects.

In CVD-deposited SiNx, the silicon content of the film can be easily tuned by changing the flow rates of relevant precursor gases within the chamber and by tuning the deposition parameters to produce high quality films. In recent years, conventional silicon-rich nitride (SRN:H) based nonlinear optics has become a popular field of study, spawning a number of works leveraging both LPCVD [39, 45, 101] and PECVD [44, 47, 102], including the demonstration of high spectro-temporal compression [103], broadband parametric amplifiers [102] as well as supercontinuum generation [52, 101] and high-speed data processing in the nonlinear regime [46].

Demonstrated applications of SRN:H stand to benefit from the use of SRN:D due to the back-end CMOS-compatible fabrication process and reduced loss when compared to PECVD SRN:H. Although LPCVD SRN:H has been observed contain lower losses compared to their PECVD counterparts,

reported refractive indexes also tend to be much lower despite high DCS:N₂ gas ratios, hovering around $2.2 \le n \le 2.3$ at the higher end [39]. By virtue of Eqs. (5)-(7), this lower refractive index has also translated to much lower values of the nonlinear parameter γ observed in LPCVD devices (n =2.2, $\gamma = 6~{\rm W}^{-1}~{\rm m}^{-1}$, $n_2 = 1.4 \times 10^{-18}~{\rm m}^2/{\rm W}$ [45]) as opposed to PECVD-based SRN:H (n = 3.1, $\gamma = 550 \text{ W}^{-1} \text{ m}^{-1}$, $n_2 = 2.8$ \times 10⁻¹⁷ [47]). The limits on the refractive index seem to be contingent on the type of deposition employed and not the precursor gases, as SRN:H devices deposited using DCS and N₂ gas have also been demonstrated to achieve a refractive index close to 3.1 [51].

Given the discussed shortcomings of that exist for LPCVD and PECVD SRN:H devices, one can see that there exists a need for a back-end CMOS-compatible material with high nonlinearity and low material absorption losses, which can be filled by high-quality SRN:D films. SRN:D devices have been demonstrated to retain the same tuneable film characteristics as has been observed in SRN:H; namely, the PECVD-deposited films are easily tuneable by changing the precursor gas ratios within the chamber. To date, SRN:D films have been realised with refractive indexes ranging

Table 4: Optical properties of SRN:D films reported in literature.

D. C	C'D N	0)4/ l
Refractive index	SiD ₄ :N ₂ gas ratio	Optical bandgap	Work, year
2.34	2:250	2.02 eV	[76], 2022
2.46	3:250	1.94 eV	[65], 2022
2.52	4:250	1.92 eV	[76], 2022

from 2.34 to 2.52, using $\mathrm{SiD_4}$: $\mathrm{N_2}$ gas ratios ranging from 1:125 to 2:125 [65, 76, 104] (Table 4). Predictions by Miller's rule have also held true for linear optical parameters where increased refractive indexes and lowered optical bandgap of the films correlated with the input gas ratios.

Presently, the dominant source of losses in SRN:D devices is observed to arise from sidewall roughness [65], which is evidenced by the exponentially decreasing loss performance of fabricated waveguides, ranging from 8 dB/cm

to 1.5 dB/cm with increasing waveguide widths (Figure 8(a)). When compared to SRN:H devices fabricated using identical fabrication techniques, the benefits of using SiD4 are easily observable in the ~2 dB/cm loss improvement at wider waveguide widths, and the contribution of parasitic hydrogen bonds in SRN:H that lead to an erratic variation of the waveguide propagation losses (Figure 8(b)). MRRs with intrinsic quality factor as high as 127,000 in the TE₀₀ mode (Figure 7(d)) and 118,000 in the TM_{00} mode have also been achieved, which are fairly comparable to LPCVD SRN:H MRRs in literature despite the higher achieved refractive index of the SRN:D film [39]. The latent 1.5 dB/cm loss within the devices could possibly be attributed to silicon clusters within the film that act as scattering centres for propagating light. These clusters have been observed in silicon-rich films [39, 45, 53] and can greatly hamper device performance in the linear regime by acting as scattering centres or as twophoton absorption sources in the presence of high intensity light.

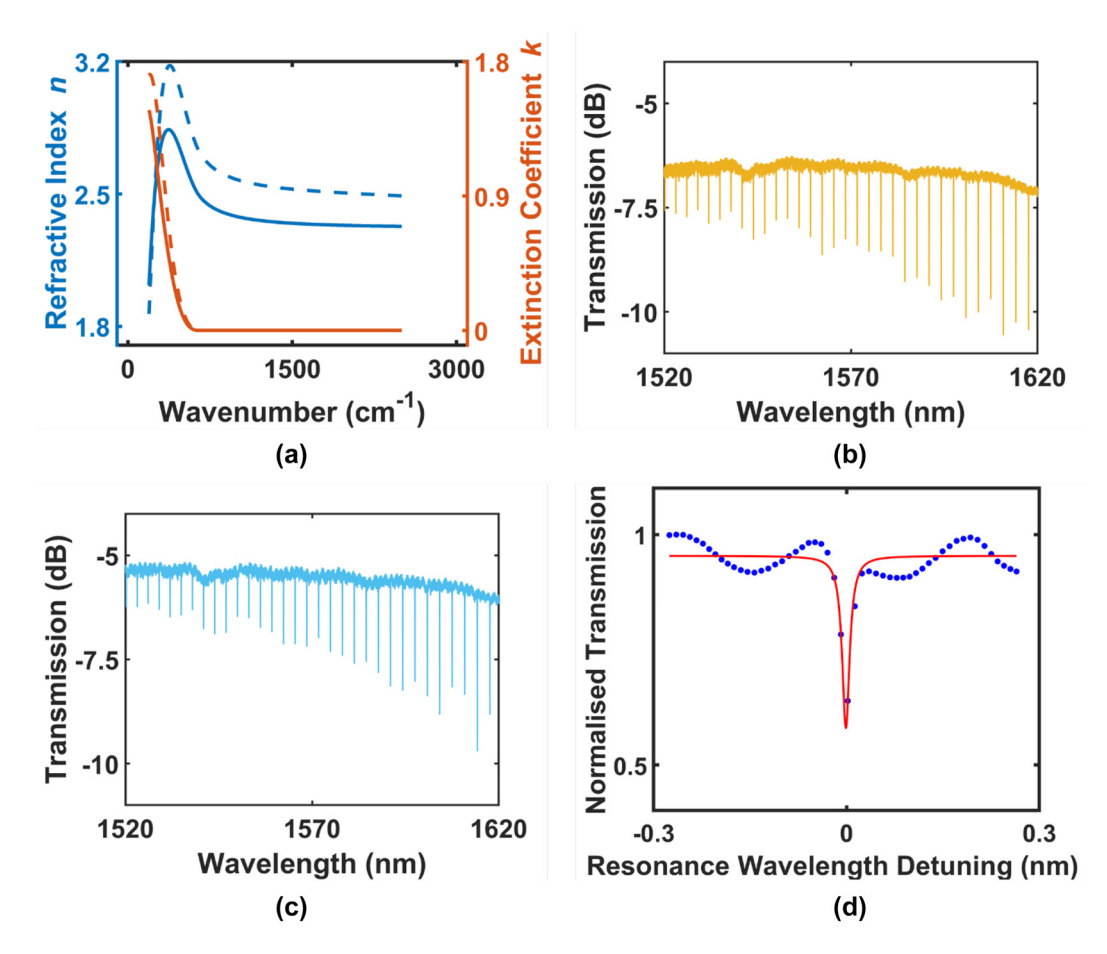


Figure 7: Characterisation results from SRN:D films and fabricated microresonators. (a) Refractive index (___) and nonlinear coefficient (___) data of film A (solid lines) and film B (dotted lines) determined using FTIR spectroscopic ellipsometry, (b) measured TE mode transmission of an MRR on the SRN:D film with refractive index n = 2.34 and (c) measured TM mode transmission spectrum of an MRR on the film with n = 2.52. Both resonators have a ring radius of 50 μ m and ring width of 1 μ m, (d) Lorentzian fit (___) and experimentally measured transmission spectrum (\bullet) of a characteristic dip in the transmission spectrum of a ring resonator with an intrinsic quality factor of 127,000 in TE mode. Figure adapted from [76].

SRN:D films and devices have also been characterised for their nonlinear optical properties [65]. In this work, the platform was fabricated using a precursor gas ratio of 3:250 (SiD₄:N₂) and was measured to have a linear refractive index of 2.46. Devices fabricated were observed to possess a nonlinear parameter $\gamma = 95 \text{ W}^{-1} \text{ m}^{-1}$ using selfphase modulation experiments, where the nonlinear phase shift of input pulses was recorded and plotted against the peak input power P_0 (Figure 8(d)). Subsequent simulations of the modal area allowed for the calculation of the film Kerr nonlinearity of $n_2 = 9.8 \times 10^{-18}$. This is roughly 35 times as high as stoichiometric SiN devices, and the films are confirmed to retain an optical bandgap above the twophoton absorption threshold of 1.6 eV. Propagation losses determined using cutback measurements are 2-2.5 dB/cm lower compared to reference SRN:H devices that were

prepared using the same recipe but with SiH₄ gas instead of SiD₄ gas.

The increased nonlinearity of SRN:D films offer the potential of enhanced nonlinear effects over current SiN:D devices. As noted in Section 3.1, frequency combs and MRR-generated solitons from a continuous-wave input are research areas that are presently in high demand, not least because of the widespread potential that these devices possess. Thus far, however, the demonstration of frequency combs in SRN:H has been guite elusive, with only a handful of works successfully demonstrating frequency combs on platforms with a Kerr nonlinearity 3-4 times above stoichiometric SiN [36, 105, 106]. Notably, these films are fabricated with LPCVD and reactive sputtering, with little mention of PECVD-deposited devices due to the high hydrogen content that makes it difficult to lock resonances in SRN:H MRRs.

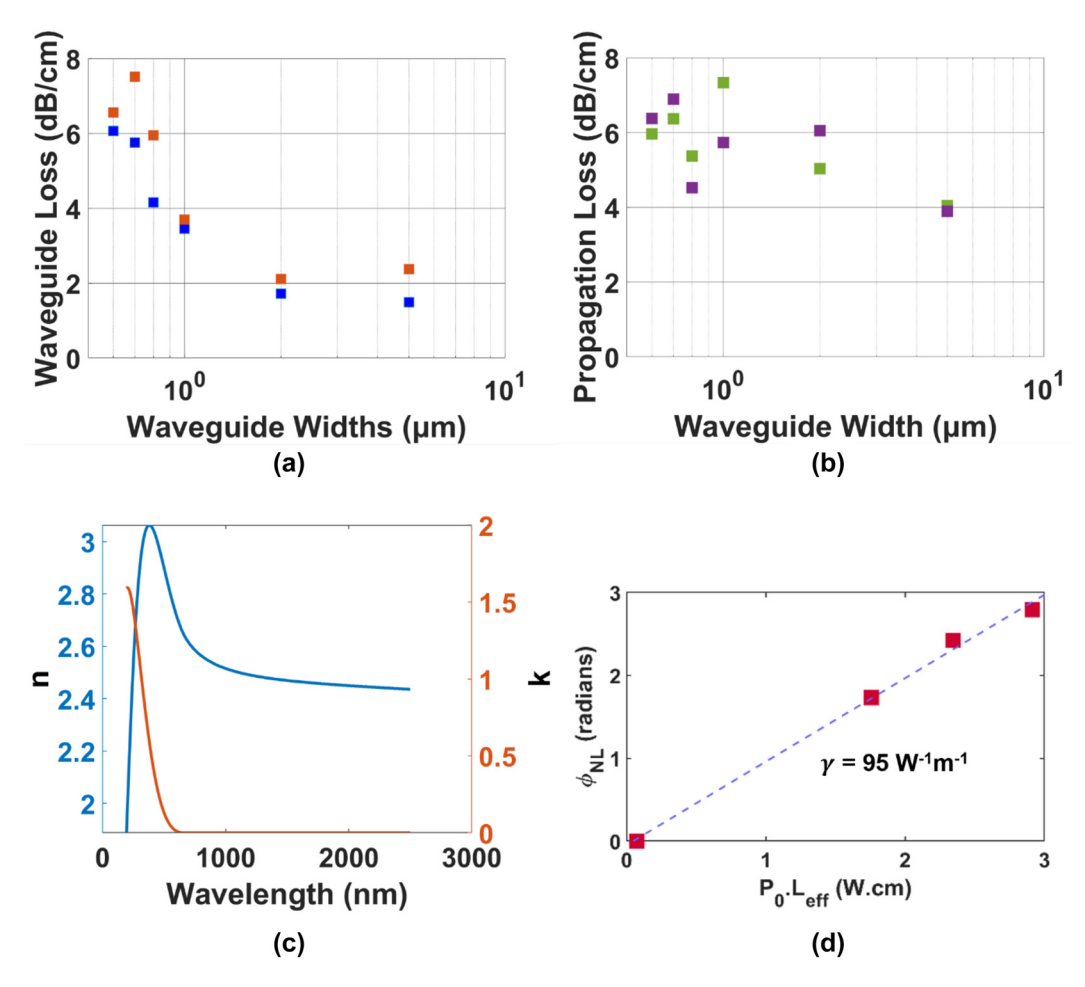


Figure 8: Characterisation results of waveguides fabricated on an SRN:D film with a refractive index of n = 2.46 at 1550 nm. (a) Waveguide propagation losses from cutback measurements on an SRN:D platform deposited with a SiD4:N2 gas ratio of 3:250 for TE 🔳 and TM 🔳 modes (b) and on an SRN:H platform (fabricated using SiH4) for TE (III) and TM (III) modes. Recipe used for SRN:H deposition is identical to that of Figure 8(a). (c) Refractive index (___) and extinction coefficient (___) of the PECVD SRN:D film, determined using spectroscopic ellipsometry, showing a linear refractive index of 2.46 at 1.55 μm. (d) Nonlinear parameter fit (...) of the experimentally determined nonlinear phase shift (...) observed in self-phase modulation experiments across different pump powers. The extracted nonlinear parameter is $95 \, \mathrm{W}^{-1} \, \mathrm{m}^{-1}$. Figure adapted from [65].

Current successes in SiN:D soliton combs and high-quality factor SRN:D MRRs should be seen as promising signs for demonstrations of soliton microcombs in highly nonlinear SRN:D devices in the near future.

4 Conclusion and future outlook

Today's state of the art low-loss nonlinear photonic devices in silicon nitride are largely fabricated using high temperature LPCVD followed by several hours of annealing at temperatures of up to 1200 °C. In certain cases, multiple wing steps are adopted [107]. The high temperatures used aim to eliminate Si-H bonds and their associated absorption. This same phenomenon - that using deuterated silane in place of regular silane eliminates - may be achieved at significantly lower temperature (<400 °C) chemical vapour deposition processes, potentially making ultra-low-loss SiNx available as a back-end CMOS-compatible process. Consequently, demonstrations of SiNx:D PICs have increased in frequency since their emergence and stand to become more common as they are leveraged for their low-loss, CMOS-compatible properties, their nonlinear functionalities potentially extended by increasing the silicon content to achieve silicon-rich films.

Further advancements in the platform could yield even lower losses. For example, the loss of high-confinement waveguides and MRRs fabricated on the platform stand to be improved through the use of an SiO₂:D cladding instead of conventional SiO₂, which will push the propagation loss lower than 0.1 dB/cm observed in Ref. [70]. Improvements in device fabrication in SRN:D films such as [65] could also greatly lower the susceptibility of Si-rich waveguides towards scattering losses due to sidewall roughness. Deposition methods and process refinements that reduce the incidence of Si nanocluster formation could also be studied to improve the quality of films. The back-end CMOS compatibility of the material opens up opportunities for electrical integration such as the placement of microheaters for onchip thermo-optic applications [108] that were previously inefficient with SRN:H devices.

One important potential implication of high-quality, low-loss, low-temperature SiNx:D platforms is their more straightforward, seamless integration with on-chip systems, which also require application specific integrated circuits (ASICs). In these systems, such as silicon photonics based [109-111], the typical process flow requires ASICs to be defined on the front end (high thermal budget), whereas photonics are defined on the back-end, which has a low thermal budget typically below 450 °C. For frequency comb-based devices to become mainstream and applicable to a wide swath of applications, not limited to data centre communications and telecommunications. lower thermal budgets than those required in LPCVDbased silicon nitride devices are required. SiNx:D could play an instrumental role in filling this gap, enabling efficient nonlinear optical functions to become more widely adopted.

Currently, demonstrated applications in SiNx:D have largely concentrated around the realisation of broadband nonlinear effects such as frequency combs and supercontinuum generation, as well as soliton generation. With the significant progress made in the SiNx:D platform to date, the development of other important nonlinear optics functions including high gain parametric amplifiers and ultrafast optical switches could be on the horizon. Nonlinear devices using SiNx:D, for example, would perform significantly better than other BEOL CMOS-compatible alternatives such as crystalline or amorphous silicon, which possess twophoton and free-carrier absorption, limiting their temporal response or achievable gain in the case of parametric amplifiers. With further development, their use could be extended to wider domains, which leverage nonlinear optical phenomena such as quantum information processing and microwave photonics. Lastly, the vast majority of work on SiNx:D thus far has focused on the Kerr effect. However, studies into other nonlinear optical effects such as its Raman response [72], potential for Brillouin scattering [112] and potentially presence (or inducement) of a $\chi^{(2)}$ response [113] could reveal even greater utility for the SiNx:D platform for nonlinear optics.

In conclusion, the SiNx:D platform has been shown to be effective in creating low-loss, low thermal budget devices with good and efficient demonstrations of nonlinear optics functions thus far. Its strong potential to provide an alternative to high thermal budget devices used today in a plethora of nonlinear optics functions is of great importance and its development timely. Future developments in both the SiNx:D platform and devices developed from it could yield new innovations, importantly not constrained by process, as well as drive their proliferation into commercial applications.

Acknowledgments: Funding from the A*STAR MTC grant (M21K2c0119), Ministry of Education ACRF Tier 2 Grant and A*STAR funding is gratefully acknowledged.

Author contributions: All the authors have accepted responsibility for the entire content of this submitted manuscript and approved submission.

Research funding: This work was supported by Ministry of Education – Singapore (ACRF Tier 2 Grant) and Agency for Science, Technology and Research (MTC Grant).

Conflict of interest statement: The authors declare no conflicts of interest regarding this article.

References

- [1] F. Duerinckx and J. Szlufcik, "Defect passivation of industrial multicrystalline solar cells based on PECVD silicon nitride," Sol. Energy Mater. Sol. Cells, vol. 72, no. 1, pp. 231-246, 2002.
- [2] A. G. Aberle and R. Hezel, "Progress in low-temperature surface passivation of silicon solar cells using remote-plasma silicon nitride," *Prog. Photovolt.: Res. Appl.*, vol. 5, no. 1, pp. 29 – 50, 1997.
- [3] A. Kaushik, H. Kahn, and A. H. Heuer, "Wafer-level mechanical characterization of silicon nitride MEMS," J. Microelectromech. Syst., vol. 14, no. 2, pp. 359-367, 2005.
- [4] R. L. Edwards, G. Coles, and W. N. Sharpe, "Comparison of tensile and bulge tests for thin-film silicon nitride," Exp. Mech., vol. 44, no. 1, pp. 49-54, 2004.
- [5] E. Cianci, A. Coppa, and V. Foglietti, "Young's modulus and residual stress of DF PECVD silicon nitride for MEMS free-standing membranes," Microelectron. Eng., vol. 84, no. 5, pp. 1296-1299, 2007.
- [6] B. M. Zwickl, W. E. Shanks, A. M. Jayich, et al., "High quality mechanical and optical properties of commercial silicon nitride membranes," Appl. Phys. Lett., vol. 92, no. 10, p. 103125, 2008.
- [7] A. Frigg, A. Boes, G. Ren, et al., "Low loss CMOS-compatible silicon nitride photonics utilizing reactive sputtered thin films," Opt. Express, vol. 27, no. 26, pp. 37795 – 37805, 2019.
- [8] B. Ding, X. Yu, H. Lu, et al., "Third-order optical nonlinearity in silicon nitride films prepared using magnetron sputtering and application for optical bistability," J. Appl. Phys., vol. 125, no. 11, p. 113102, 2019.
- [9] K. Ikeda, R. E. Saperstein, N. Alic, and Y. Fainman, "Thermal and Kerr nonlinear properties of plasma-deposited silicon nitride/silicon dioxide waveguides," Opt. Express, vol. 16, no. 17, pp. 12987-12994, 2008.
- [10] D. T. H. Tan, K. Ikeda, P. C. Sun, and Y. Fainman, "Group velocity dispersion and self phase modulation in silicon nitride waveguides," Appl. Phys. Lett., vol. 96, no. 6, p. 061101, 2010.
- [11] T. J. Kippenberg, R. Holzwarth, and S. A. Diddams, "Microresonator-based optical frequency combs," Science, vol. 332, no. 6029, pp. 555-559, 2011.
- [12] Y. Okawachi, K. Saha, J. S. Levy, Y. H. Wen, M. Lipson, and A. L. Gaeta, "Octave-spanning frequency comb generation in a silicon nitride chip," Opt. Lett., vol. 36, no. 17, pp. 3398 – 3400,
- [13] T. Herr, K. Hartinger, J. Riemensberger, et al., "Universal formation dynamics and noise of Kerr-frequency combs in microresonators," Nat. Photonics, vol. 6, no. 7, pp. 480-487, 2012.
- [14] T. Herr, V. Brasch, J. D. Jost, et al., "Temporal solitons in optical microresonators," Nat. Photonics, vol. 8, no. 2, pp. 145-152, 2014.
- [15] V. Brasch, M. Geiselmann, T. Herr, et al., "Photonic chip based optical frequency comb using soliton Cherenkov radiation," Science, vol. 351, no. 6271, pp. 357-360, 2016.
- [16] M. H. P. Pfeiffer, C. Herkommer, J. Liu, et al., "Octave-spanning dissipative Kerr soliton frequency combs in Si3N4 microresonators," Optica, vol. 4, no. 7, pp. 684-691, 2017.

- [17] H. Guo, M. Karpov, E. Lucas, et al., "Universal dynamics and deterministic switching of dissipative Kerr solitons in optical microresonators," Nat. Phys., vol. 13, no. 1, pp. 94-102, 2017.
- [18] S. W. Huang, J. Yang, S. H. Yang, et al., "Globally stable microresonator turing pattern formation for coherent high-power THz radiation on-chip," Phys. Rev. X, vol. 7, no. 4, p. 041002, 2017.
- [19] T. J. Kippenberg, A. L. Gaeta, M. Lipson, and M. L. Gorodetsky, "Dissipative Kerr solitons in optical microresonators," Science, vol. 361, no. 6402, p. eaan8083, 2018.
- [20] M. Karpov, M. H. P. Pfeiffer, H. Guo, W. Weng, J. Liu, and T. J. Kippenberg, "Dynamics of soliton crystals in optical microresonators," Nat. Phys., vol. 15, no. 10, pp. 1071-1077, 2019.
- [21] P. Marin-Palomo, J. N. Kemal, M. Karpov, et al., "Microresonator-based solitons for massively parallel coherent optical communications," *Nature*, vol. 546, no. 7657, pp. 274 – 279, 2017.
- [22] A. Fülöp, M. Mazur, A. Lorences-Riesgo, et al., "High-order coherent communications using mode-locked dark-pulse Kerr combs from microresonators," Nat. Commun., vol. 9, no. 1, p. 1598, 2018.
- [23] H. Hu, F. Da Ros, M. Pu, et al., "Single-source chip-based frequency comb enabling extreme parallel data transmission," *Nat. Photonics*, vol. 12, no. 8, pp. 469 – 473, 2018.
- [24] A. S. Raja, S. Lange, M. Karpov, et al., "Ultrafast optical circuit switching for data centers using integrated soliton microcombs," Nat. Commun., vol. 12, no. 1, p. 5867, 2021.
- [25] P. Xing, G. F. Chen, H. Gao, et al., "Microresonator frequency comb based high-speed transmission of intensity modulated direct detection data," Nanophotonics, vol. 11, no. 14, pp. 3269-3280, 2022.
- [26] S. B. Papp, K. Beha, P. Del'Haye, et al., "Microresonator frequency comb optical clock," Optica, vol. 1, no. 1, pp. 10-14, 2014.
- [27] S. W. Huang, J. Yang, M. Yu, et al., "A broadband chip-scale optical frequency synthesizer at 2.7×10^{-16} relative uncertainty," Sci. Adv., vol. 2, no. 4, p. e1501489, 2016.
- [28] A. Dutt, C. Joshi, X. Ji, et al., "On-chip dual-comb source for spectroscopy," Sci. Adv., vol. 4, no. 3, p. e1701858, 2018.
- [29] D. T. Spencer, T. Drake, T. C. Briles, et al., "An optical-frequency synthesizer using integrated photonics," Nature, vol. 557, no. 7703, pp. 81-85, 2018.
- [30] L. Stern, J. R. Stone, S. Kang, et al., "Direct Kerr frequency comb atomic spectroscopy and stabilization," Sci. Adv., vol. 6, no. 9, p. eaax6230, 2020.
- [31] D. J. Blumenthal, R. Heideman, D. Geuzebroek, A. Leinse, and C. Roeloffzen, "Silicon nitride in silicon photonics," Proc. IEEE, vol. 106, no. 12, pp. 2209-2231, 2018.
- [32] J. F. Bauters, M. J. R. Heck, D. John, et al., "Ultra-low-loss high-aspect-ratio Si3N4 waveguides," Opt. Express, vol. 19, no. 4, pp. 3163 - 3174, 2011.
- [33] J. F. Bauters, M. J. R. Heck, D. D. John, et al., "Planar waveguides with less than 0.1 dB/m propagation loss fabricated with wafer bonding," Opt. Express, vol. 19, no. 24, pp. 24090 – 24101, 2011.
- [34] J. F. Bauters, M. L. Davenport, M. J. R. Heck, et al., "Silicon on ultra-low-loss waveguide photonic integration platform," Opt. Express, vol. 21, no. 1, pp. 544-555, 2013.
- [35] X. Ji, F. A. S. Barbosa, S. P. Roberts, et al., "Ultra-low-loss on-chip resonators with sub-milliwatt parametric oscillation threshold," *Optica*, vol. 4, no. 6, pp. 619 – 624, 2017.

- [36] Z. Ye, A. Fülöp, Ó. B. Helgason, P. A. Andrekson, and V. Torres-Company, "Low-loss high-Q silicon-rich silicon nitride microresonators for Kerr nonlinear optics," Opt. Lett., vol. 44, no. 13, pp. 3326 – 3329, 2019.
- [37] J. Liu, G. Huang, R. N. Wang, et al., "High-yield, wafer-scale fabrication of ultralow-loss, dispersion-engineered silicon nitride photonic circuits," Nat. Commun., vol. 12, no. 1, p. 2236, 2021.
- [38] O. Debieu, R. P. Nalini, I. Cardin, X. Portier, I. Perrière, and F. Gourbilleau, "Structural and optical characterization of pure Si-rich nitride thin films," Nanoscale Res. Lett., vol. 8, no. 1, p. 31,
- [39] C. J. Krückel, A. Fülöp, T. Klintberg, J. Bengtsson, P. A. Andrekson, and V. Torres-Company, "Linear and nonlinear characterization of low-stress high-confinement silicon-rich nitride waveguides," Opt. Express, vol. 23, no. 20, pp. 25827-25837, 2015.
- [40] M. Mitrovic, X. Guan, H. Ji, L. K. Oxenløwe, and L. H. Frandsen, "Four-wave mixing in silicon-rich nitride waveguides," in Frontiers in Optics 2015, San Jose, California, Optica Publishing Group, OSA Technical Digest (online), 2015, p. FM1D.6 [Online]. Available at: https://opg.optica.org/abstract.cfm?URI=FiO-2015-FM1D.6.
- [41] C. L. Wu, Y. H. Lin, S. P. Su, et al., "Enhancing optical nonlinearity in a nonstoichiometric SiN waveguide for cross-wavelength all-optical data processing," ACS Photonics, vol. 2, no. 8, pp. 1141-1154, 2015.
- [42] G. R. Lin, S. P. Su, C. L. Wu, et al., "Si-rich SiNx based Kerr switch enables optical data conversion up to 12 Gbit/s," Sci. Rep., vol. 5, no. 1, p. 9611, 2015.
- [43] M. W. Puckett, R. Sharma, H. H. Lin, M. H. Yang, F. Vallini, and Y. Fainman, "Observation of second-harmonic generation in silicon nitride waveguides through bulk nonlinearities," Opt. Express, vol. 24, no. 15, pp. 16923-16933, 2016.
- [44] C. Lacava, S. Stankovic, A. Z. Khokhar, et al., "Si-Rich silicon nitride for nonlinear signal processing applications," Sci. Rep., vol. 7, no. 1, p. 22, 2017.
- [45] C. J. Krückel, A. Fülöp, Z. Ye, P. A. Andrekson, and V. Torres-Company, "Optical bandgap engineering in nonlinear silicon nitride waveguides," Opt. Express, vol. 25, no. 13, pp. 15370-15380, 2017.
- [46] M. R. Dizaji, C. J. Krückel, A. Fülöp, P. A. Andrekson, V. Torres-Company, and L. R. Chen, "Silicon-rich nitride waveguides for ultra-broadband nonlinear signal processing," Opt. Express, vol. 25, no. 11, pp. 12100-12108, 2017.
- [47] K. J. A. Ooi, D. K. T. Ng, T. Wang, et al., "Pushing the limits of CMOS optical parametric amplifiers with USRN:Si7N3 above the two-photon absorption edge," Nat. Commun., vol. 8, no. 1, p. 13878, 2017.
- [48] C. Yang and J. Pham, "Characteristic study of silicon nitride films deposited by LPCVD and PECVD," Silicon, vol. 10, no. 6, pp. 2561-2567, 2018.
- [49] D. T. H. Tan, K. J. A. Ooi, and D. K. T. Ng, "Nonlinear optics on silicon-rich nitride—a high nonlinear figure of merit CMOS platform [Invited]," Photonics Res., vol. 6, no. 5, pp. B50-B66,
- [50] A. Friedman, H. Nejadriahi, R. Sharma, and Y. Fainman, "Demonstration of the DC-Kerr effect in silicon-rich nitride," Opt. Lett., vol. 46, no. 17, pp. 4236 – 4239, 2021.
- [51] D. K. T. Ng, H. Gao, P. Xing, et al., "Enhanced photonics devices based on low temperature plasma-deposited

- dichlorosilane-based ultra-silicon-rich nitride (Si8N)," Sci. Rep., vol. 12, no. 1, p. 5267, 2022.
- [52] T. Wang, D. K. T. Ng, S. K. Ng, et al., "Supercontinuum generation in bandgap engineered, back-end CMOS compatible silicon rich nitride waveguides," Laser Photonics Rev., vol. 9, no. 5, pp. 498-506, 2015.
- [53] I. Guler, "Optical and structural characterization of silicon nitride thin films deposited by PECVD," Mater. Sci. Eng. B, vol. 246, pp. 21-26, 2019.
- [54] S. C. Mao, S. H. Tao, Y. L. Xu, et al., "Low propagation loss SiN optical waveguide prepared by optimal low-hydrogen module," Opt. Express, vol. 16, no. 25, pp. 20809 - 20816, 2008.
- [55] F. Ay and A. Aydinli, "Comparative investigation of hydrogen bonding in silicon based PECVD grown dielectrics for optical waveguides," Opt. Mater., vol. 26, no. 1, pp. 33-46, 2004.
- [56] T. Hiraki, T. Aihara, H. Nishi, and T. Tsuchizawa, "Deuterated SiN/SiON waveguides on Si platform and their application to C-band WDM filters," *IEEE Photonics J.*, vol. 9, no. 5, pp. 1–7, 2017.
- [57] J. Yota, J. Hander, and A. A. Saleh, "A comparative study on inductively-coupled plasma high-density plasma, plasma-enhanced, and low pressure chemical vapor deposition silicon nitride films," J. Vac. Sci. Technol., A, vol. 18, no. 2, pp. 372-376, 2000.
- [58] M. Maeda and H. Nakamura, "Infrared spectroscopic study of hydrogenated and deuterated silicon nitride films prepared from plasma-enhanced deposition," J. Appl. Phys., vol. 55, no. 8, pp. 3068 - 3071, 1984.
- [59] M. H. P. Pfeiffer, A. Kordts, V. Brasch, et al., "Photonic Damascene process for integrated high-Q microresonator based nonlinear photonics," Optica, vol. 3, no. 1, pp. 20-25, 2016.
- [60] M. H. P. Pfeiffer, C. Herkommer, J. Liu, et al., "Photonic damascene process for low-loss, high-confinement silicon nitride waveguides," IEEE J. Sel. Top. Quantum Electron., vol. 24, no. 4, nn. 1-11. 2018.
- [61] Z. Ye, K. Twayana, P. A. Andrekson, and V. Torres-Company, "High-Q Si3N4 microresonators based on a subtractive processing for Kerr nonlinear optics," Opt. Express, vol. 27, no. 24, pp. 35719 - 35727, 2019.
- [62] X. Ji, Y. Okawachi, A. Gil-Molina, et al., "Ultra-low-loss silicon nitride photonics based on deposited films compatible with foundries," Laser Photonics Rev., p. 2200544, 2023, https://doi.org/ 10.1002/lpor.202200544.
- [63] S. Sedky, A. Witvrouw, H. Bender, and K. Baert, "Experimental determination of the maximum post-process annealing temperature for standard CMOS wafers," IEEE Trans. Electron Devices, vol. 48, no. 2, pp. 377-385, 2001.
- [64] Y. Son, B. Frost, Y. Zhao, and R. L. Peterson, "Monolithic integration of high-voltage thin-film electronics on low-voltage integrated circuits using a solution process," Nat. Electron., vol. 2, no. 11, pp. 540 – 548, 2019.
- [65] X. X. Chia, G. F. R. Chen, Y. Cao, et al., "Optical characterization of deuterated silicon-rich nitride waveguides," Sci. Rep., vol. 12, no. 1, p. 12697, 2022.
- [66] P. Atkins and J. De Paula, Physical Chemistry, Oxford, Oxford University Press, 2006.
- [67] Z. Wu, Y. Zhang, S. Zeng, et al., "Low-noise Kerr frequency comb generation with low temperature deuterated silicon nitride waveguides," Opt. Express, vol. 29, no. 18, pp. 29557-29566, 2021.

- [68] D. Bose, J. Wang, and D. J. Blumenthal, "250C process for < 2dB/m ultra-low loss silicon nitride integrated photonic waveguides," in Conference on Lasers and Electro-Optics, San Jose, California, Optica Publishing Group, Technical Digest Series, 2022, p. SF3O.1 [Online]. Available at: http://opg.optica.org/abstract.cfm?URI= CLEO SI-2022-SF3O.1.
- [69] J. Chiles, N. Nader, D. D. Hickstein, et al., "Deuterated silicon nitride photonic devices for broadband optical frequency comb generation," Opt. Lett., vol. 43, no. 7, pp. 1527-1530, 2018.
- [70] Y. Xie, J. Li, Y. Zhang, et al., "Soliton frequency comb generation in CMOS-compatible silicon nitride microresonators," Photonics Res., vol. 10, no. 5, pp. 1290-1296, 2022.
- [71] Z. Wu, Y. Chen, Z. Xu, et al., "Waveguide-integrated deuterated silicon nitride (SiN: D) microdisk resonators for nonlinear photonics," in Asia Communications and Photonics Conference (ACPC) 2019, Chengdu, Optica Publishing Group, OSA Technical Digest, 2019, p. M4C.7 [Online]. Available at: https://opg.optica. org/abstract.cfm?URI=ACPC-2019-M4C.7.
- [72] Z. Wu, Z. Shao, Y. Zhang, et al., "High quality factor deuterated silicon nitride (SiN:D) microring resonators," in CLEO Pacific Rim Conference 2018, Hong Kong, Optica Publishing Group, OSA Technical Digest, 2018, p. W4D.5 [Online]. Available at: http://opg.optica.org/abstract.cfm?URI=CLEOPR-2018-W4D.5.
- [73] W. Jin, D. D. John, J. F. Bauters, T. Bosch, B. J. Thibeault, and J. E. Bowers, "Deuterated silicon dioxide for heterogeneous integration of ultra-low-loss waveguides," Opt. Lett., vol. 45, no. 12, pp. 3340 - 3343, 2020.
- [74] K. Liu, N. Jun, H. Cheng, et al., "720 million quality factor integrated all-waveguide photonic resonator," in 2021 Device Research Conference (DRC), XXX, 2021, pp. 1-2.
- [75] T. Aihara, T. Hiraki, H. Nishi, T. Tsuchizawa, and S. Matsuo, "Single soliton generation with deuterated SiN ring resonator fabricated at low temperature," in Presented at the Conference on Lasers and Electro-Optics, Hokkaido, Japan, Pacific Rim, 2022. CThP12D-06.
- [76] X. X. Chia, P. Xing, J. W. Choi, and D. T. H. Tan, "High quality factor deuterated silicon-rich nitride micro-ring resonators," in *Presented* at the Conference on Lasers and Electro-Optics, Hokkaido, Japan, Pacific Rim, 2022. CThP12D-05.
- [77] Q. Zhao, M. W. Harrington, A. Isichenko, et al., "Integrated reference cavity with dual-mode optical thermometry for frequency correction," Optica, vol. 8, no. 11, pp. 1481 – 1487, 2021.
- [78] G. P. Agrawal, Nonlinear Fiber Optics, Oxford, United Kingdom, Elsevier Science, 2013.
- [79] L. A. Lugiato and R. Lefever, "Spatial dissipative structures in passive optical systems," Phys. Rev. Lett., vol. 58, no. 21, pp. 2209 - 2211, 1987.
- [80] T. Udem, R. Holzwarth, and T. W. Hänsch, "Optical frequency metrology," Nature, vol. 416, no. 6877, pp. 233-237, 2002.
- [81] I. Coddington, W. C. Swann, and N. R. Newbury, "Coherent multiheterodyne spectroscopy using stabilized optical frequency combs," Phys. Rev. Lett., vol. 100, no. 1, p. 013902, 2008.
- [82] M. A. Foster, J. S. Levy, O. Kuzucu, K. Saha, M. Lipson, and A. L. Gaeta, "Silicon-based monolithic optical frequency comb source," Opt. Express, vol. 19, no. 15, pp. 14233 – 14239, 2011.
- [83] P. Del'Haye, A. Schliesser, O. Arcizet, T. Wilken, R. Holzwarth, and T. J. Kippenberg, "Optical frequency comb generation from a monolithic microresonator," Nature, vol. 450, no. 7173, pp. 1214-1217, 2007.

- [84] Y. K. Chembo, "Kerr optical frequency combs: theory, applications and perspectives," Nanophotonics, vol. 5, no. 2, pp. 214-230,
- [85] A. Schliesser, N. Picqué, and T. W. Hänsch, "Mid-infrared frequency combs," Nat. Photonics, vol. 6, no. 7, pp. 440-449,
- [86] H. Zhang, B. Chang, Z. Li, et al., "Coherent optical frequency combs: from principles to applications," J. Electron. Sci. Technol., vol. 20, no. 2, p. 100157, 2022.
- [87] L. Chang, S. Liu, and J. E. Bowers, "Integrated optical frequency comb technologies," Nat. Photonics, vol. 16, no. 2, pp. 95-108, 2022.
- [88] D. C. Cole, E. S. Lamb, P. Del'Haye, S. A. Diddams, and S. B. Papp, "Soliton crystals in Kerr resonators," Nat. Photonics, vol. 11, no. 10, pp. 671 – 676, 2017.
- [89] M. G. Suh and K. J. Vahala, "Soliton microcomb range measurement," Science, vol. 359, no. 6378, pp. 884-887, 2018.
- [90] B. Stern, X. Ji, Y. Okawachi, A. L. Gaeta, and M. Lipson, "Battery-operated integrated frequency comb generator," *Nature*, vol. 562, no. 7727, pp. 401-405, 2018.
- [91] H. Zhou, Y. Geng, W. Cui, et al., "Soliton bursts and deterministic dissipative Kerr soliton generation in auxiliary-assisted microcavities," Light: Sci. Appl., vol. 8, no. 1, p. 50, 2019.
- [92] J. A. Jaramillo-Villegas, X. Xue, P. H. Wang, D. E. Leaird, and A. M. Weiner, "Deterministic single soliton generation and compression in microring resonators avoiding the chaotic region," Opt. Express, vol. 23, no. 8, pp. 9618 - 9626, 2015.
- [93] P. H. Wang, J. A. Jaramillo-Villegas, Y. Xuan, et al., "Intracavity characterization of micro-comb generation in the single-soliton regime," Opt. Express, vol. 24, no. 10, pp. 10890 – 10897, 2016.
- [94] X. Ji, J. K. Jang, U. D. Dave, et al., "Exploiting ultralow loss multimode waveguides for broadband frequency combs," Laser Photonics Rev., vol. 15, no. 1, p. 2000353, 2021.
- [95] J. Liu, A. S. Raja, M. Karpov, et al., "Ultralow-power chip-based soliton microcombs for photonic integration," Optica, vol. 5, no. 10, pp. 1347-1353, 2018.
- [96] T. Dai, A. Shen, G. Wang, et al., "Bandwidth and wavelength tunable optical passband filter based on silicon multiple microring resonators," Opt. Lett., vol. 41, no. 20, pp. 4807-4810, 2016.
- [97] J. G. E. Gardeniers, H. A. C. Tilmans, and C. C. G. Visser, "LPCVD silicon-rich silicon nitride films for applications in micromechanics, studied with statistical experimental design," J. Vac. Sci. Technol., A, vol. 14, no. 5, pp. 2879 – 2892, 1996.
- [98] G. New, Introduction to Nonlinear Optics, Cambridge, United Kingdom, Cambridge University Press, 2011.
- [99] R. W. Boyd, Nonlinear Optics, Cambridge, Massachusetts, USA, Academic Press, 2020.
- [100] R. C. Miller, "Optical second harmonic generation in piezoelectric crystals," Appl. Phys. Lett., vol. 5, no. 1, pp. 17-19, 1964.
- [101] X. Liu, M. Pu, B. Zhou, et al., "Octave-spanning supercontinuum generation in a silicon-rich nitride waveguide," Opt. Lett., vol. 41, no. 12, pp. 2719-2722, 2016.
- [102] M. Yang, L. Xu, J. Wang, et al., "An octave-spanning optical parametric amplifier based on a low-dispersion silicon-rich nitride waveguide," IEEE J. Sel. Top. Quantum Electron., vol. 24, no. 6, pp. 1-7, 2018.

- [103] J. W. Choi, E. Sahin, B. U. Sohn, et al., "High spectro-temporal compression on a nonlinear CMOS-chip," Light: Sci. Appl., vol. 10, no. 1, p. 130, 2021.
- [104] X. X. Chia, G. F. R. Chen, Y. M. Cao, D. K. T. Ng, P. Xing, and D. T. H. Tan, "Nonlinear optical characterization of deuterated silicon-rich nitride waveguides," in OSA Nonlinear Optics 2021, R. C. C. C. D. Boyd and P. Rakich, Eds., Washington, DC, Optica Publishing Group, OSA Technical Digest, 2021, p. NM2A.7 [Online]. Available at: http://opg.optica.org/abstract.cfm?URI= NLO-2021-NM2A.7.
- [105] A. Frigg, A. Boes, G. Ren, et al., "Optical frequency comb generation with low temperature reactive sputtered silicon nitride waveguides," APL Photonics, vol. 5, no. 1, p. 011302, 2020
- [106] S. Christensen, Z. Ye, M. Bache, and V. T. Company, "Octave-spanning frequency comb generation in all-normaldispersion silicon-rich silicon nitride waveguide," in Conference on Lasers and Electro-Optics, Washington, DC, Optica Publishing Group, OSA Technical Digest, 2020, p. STu3H.7 [Online]. Available at: https://opg.optica.org/abstract.cfm?URI=CLEO_SI-2020-STu3H.7.
- [107] A. Gondarenko, J. S. Levy, and M. Lipson, "High confinement micron-scale silicon nitride high Q ring resonator," Opt. Express, vol. 17, no. 14, pp. 11366-11370, 2009.
- [108] H. Nejadriahi, A. Friedman, R. Sharma, S. Pappert, Y. Fainman, and P. Yu, "Thermo-optic properties of silicon-rich silicon nitride for

- on-chip applications," Opt. Express, vol. 28, no. 17, pp. 24951-24960, 2020.
- [109] R. Nagarajan, M. Filer, Y. Fu, M. Kato, T. Rope, and J. Stewart, "Silicon photonics-based 100 Gbit/s, PAM4, DWDM data center interconnects," J. Opt. Commun. Netw., vol. 10, no. 7, pp. B25 - B36,
- [110] M. Traverso, M. Mazzini, K. Lakshmikumar, et al., "Integrated silicon photonics transceiver module for 100Gbit/s 20km transmission," in Optical Fiber Communication Conference (OFC) 2021, P. K. J. X. C. C. R. C. C. Dong, and M. Li, Eds., Washington, DC, Optica Publishing Group, OSA Technical Digest, 2021, p. M3A.3 [Online]. Available at: https://opg.optica.org/abstract.cfm?URI=OFC-2021-M3A.3.
- [111] S. Amiralizadeh, W. Lin, D. Patel et al., "System optimization of high-efficiency 400 Gb/s PAM4 silicon photonics transmitter for data center applications," in Optical Fiber Communication Conference (OFC) 2021, P. K. J. X. C. C. R. C. C. Dong, and M. Li, Eds., Washington, DC, Optica Publishing Group, OSA Technical Digest, 2021, p. M3A.4 [Online]. Available at: https://opg.optica.org/ abstract.cfm?URI=OFC-2021-M3A.4.
- [112] B. J. Eggleton, C. G. Poulton, P. T. Rakich, M. J. Steel, and G. Bahl, "Brillouin integrated photonics," Nat. Photonics, vol. 13, no. 10, pp. 664-677, 2019.
- [113] E. Nitiss, J. Hu, A. Stroganov, and C. S. Brès, "Optically reconfigurable quasi-phase-matching in silicon nitride microresonators," Nat. Photonics, vol. 16, no. 2, pp. 134-141, 2022.